MNRAS **000**, 000–000 (0000) Preprint 23rd August 2020 Compiled using MNRAS LATEX style file v3.0

EoS Figures

Luke Chamandy,★
Department of Physics and Astronomy, University of Rochester, Rochester NY 14627, USA

23rd August 2020

ABSTRACT
Figures

Key words: binaries: close – stars: evolution – stars: kinematics and dynamics – stars: mass loss – stars: winds, outflows – hydrodynamics

References

Ohlmann S. T., Röpke F. K., Pakmor R., Springel V., 2017, A&A, 599, A5

★ lchamandy@pas.rochester.edu

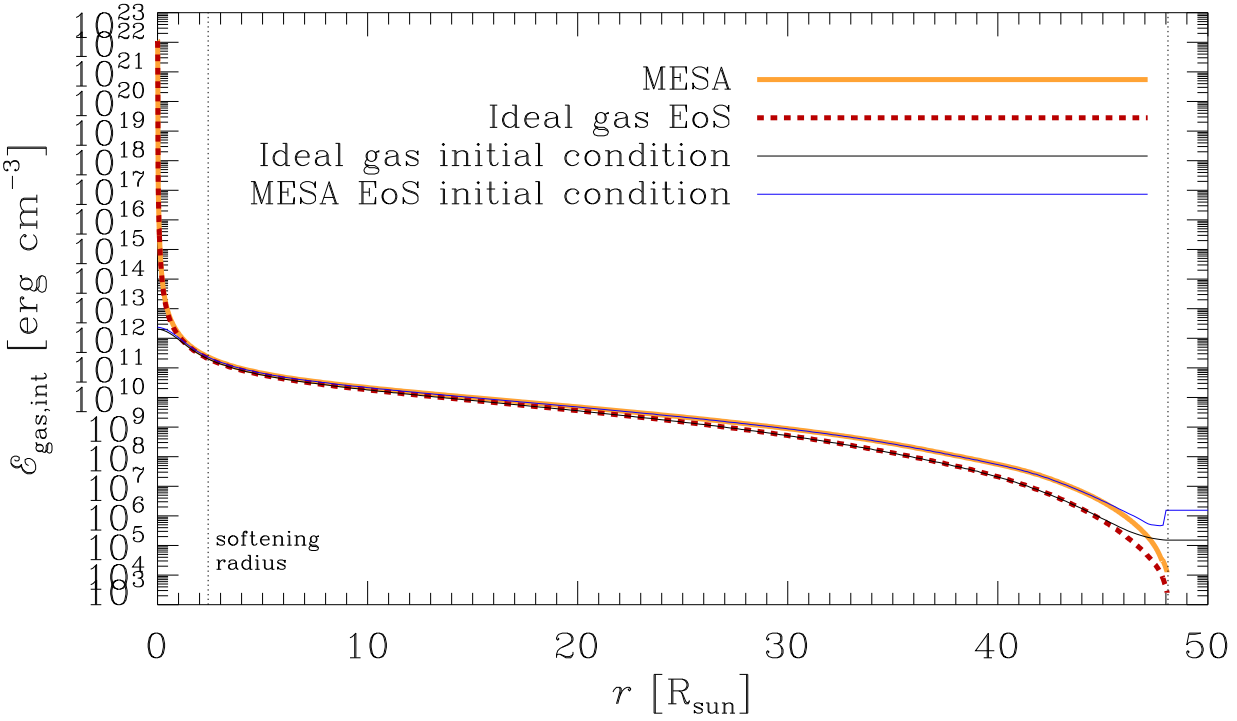

Figure 1. Comparison of internal energy density profile between MESA and simulation for Run 143 (fiducial $\gamma = 5/3$ RGB run) and Run 207 (new MESA tabular EoS run). The same MESA profile is used for both runs.

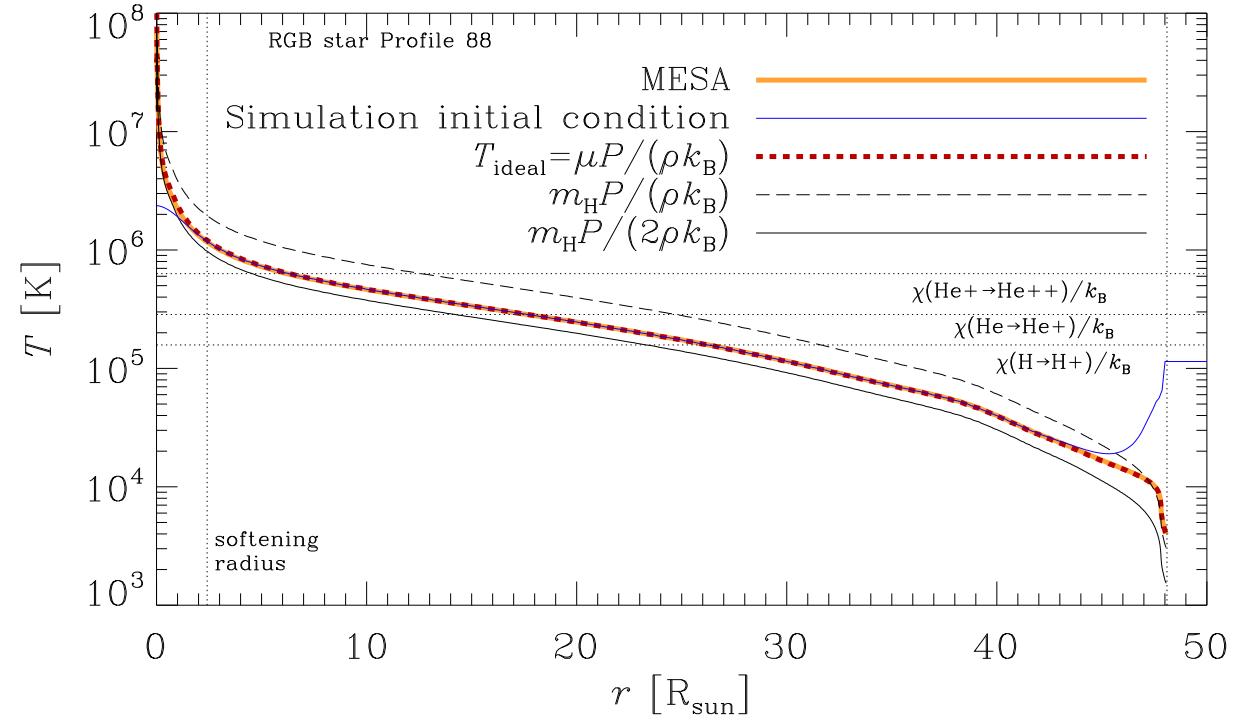

Figure 2. Temperature profile.

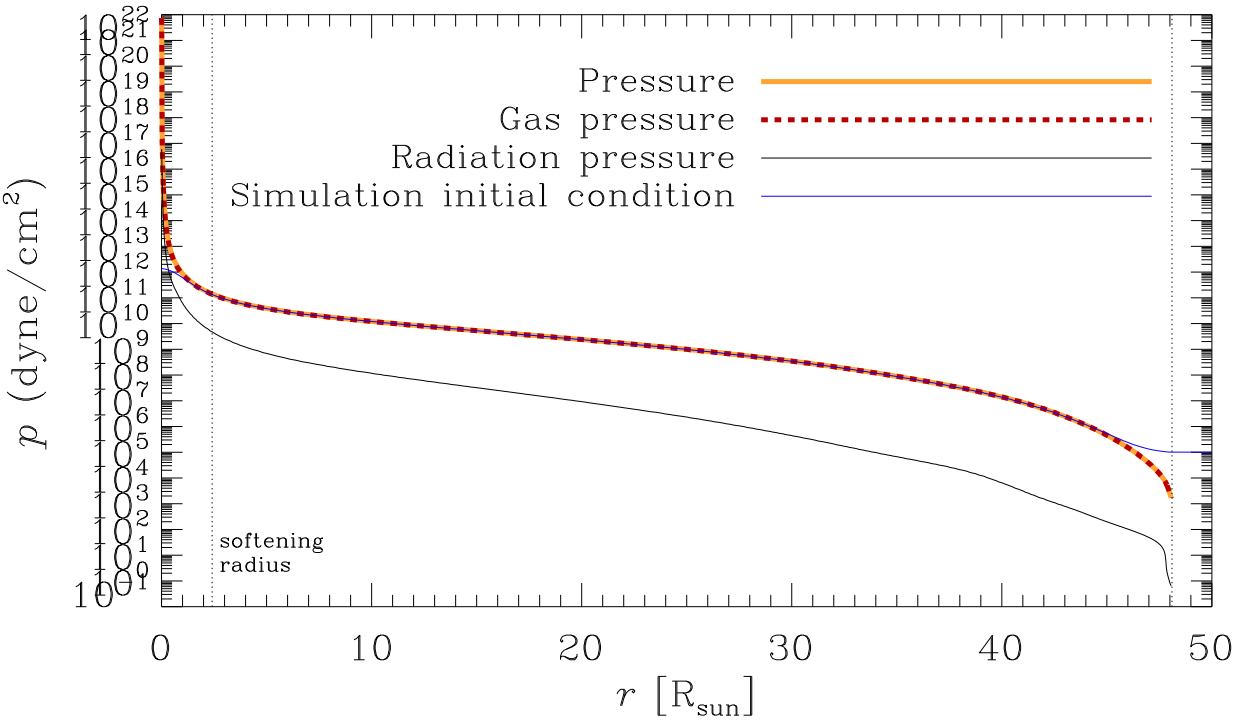

Figure 3. Pressure profile.

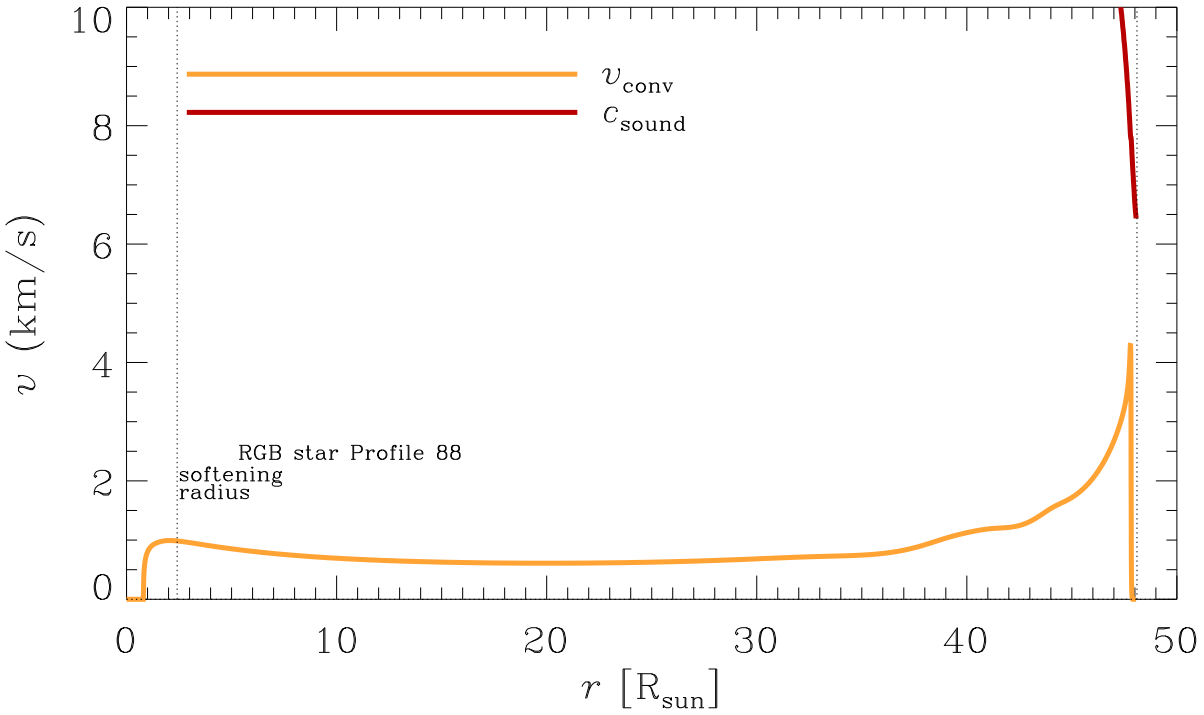

Figure 4. Convective speed from MESA along with sound speed from MESA. We see that the typical convective speed is $\sim 0.7\,\mathrm{km\,s^{-1}}$, rising to $\sim 1\,\mathrm{km\,s^{-1}}$ near the softening radius and steadily rising to $\sim 4\,\mathrm{km\,s^{-1}}$ near the surface.

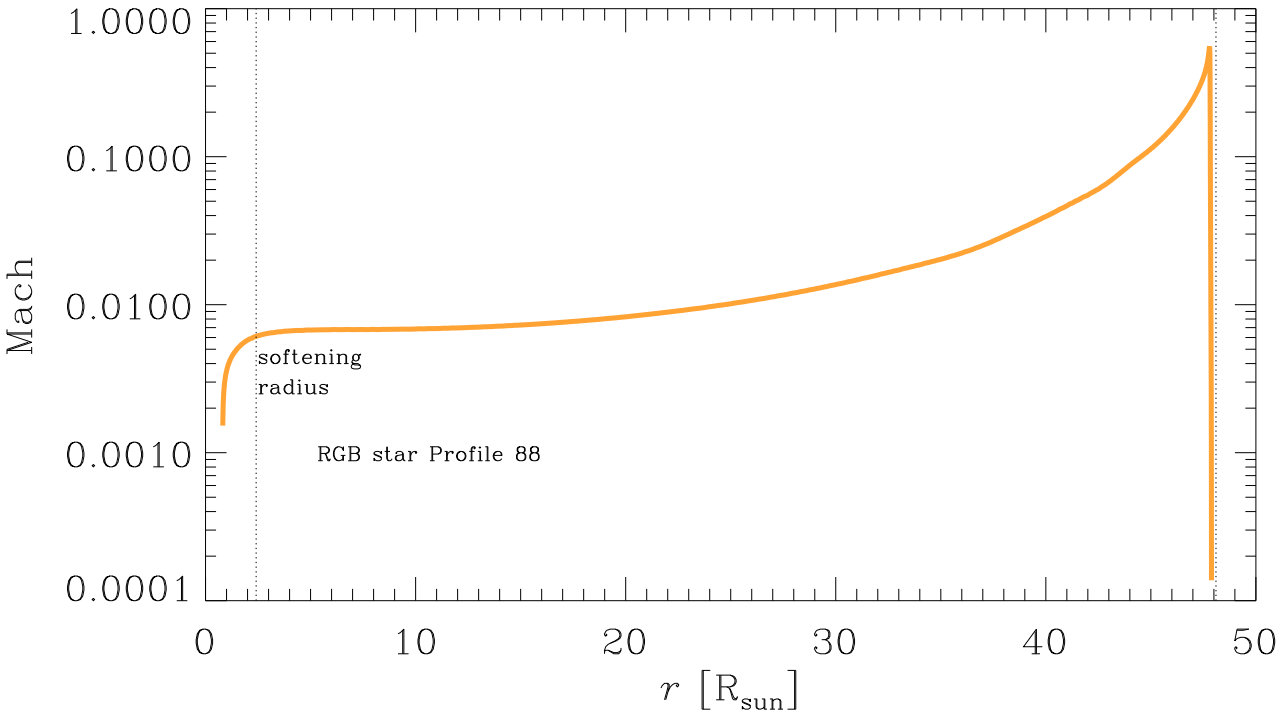

Figure 5. Mach number (convective speed divided by sound speed).

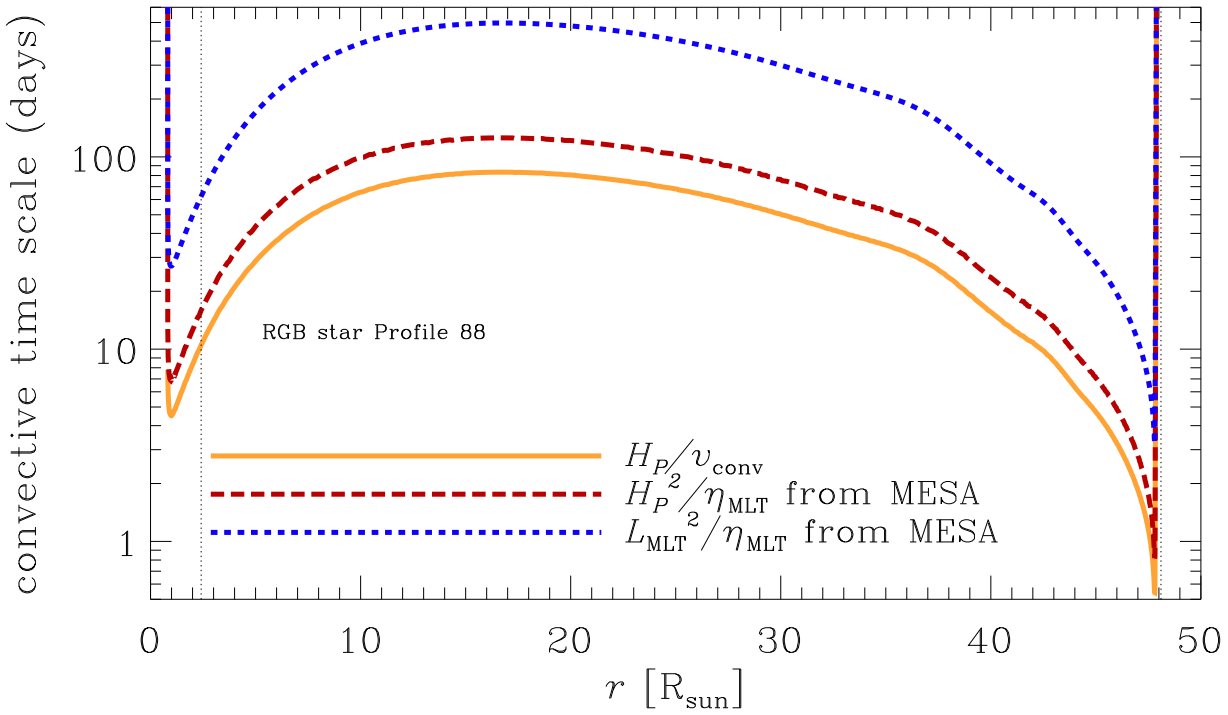

Figure 6. Convective time scale (various estimates). H_P is pressure scale height, $\eta_{\rm MLT}$ is diffusivity from mixing length theory, $L_{\rm MLT}$ is mixing length.

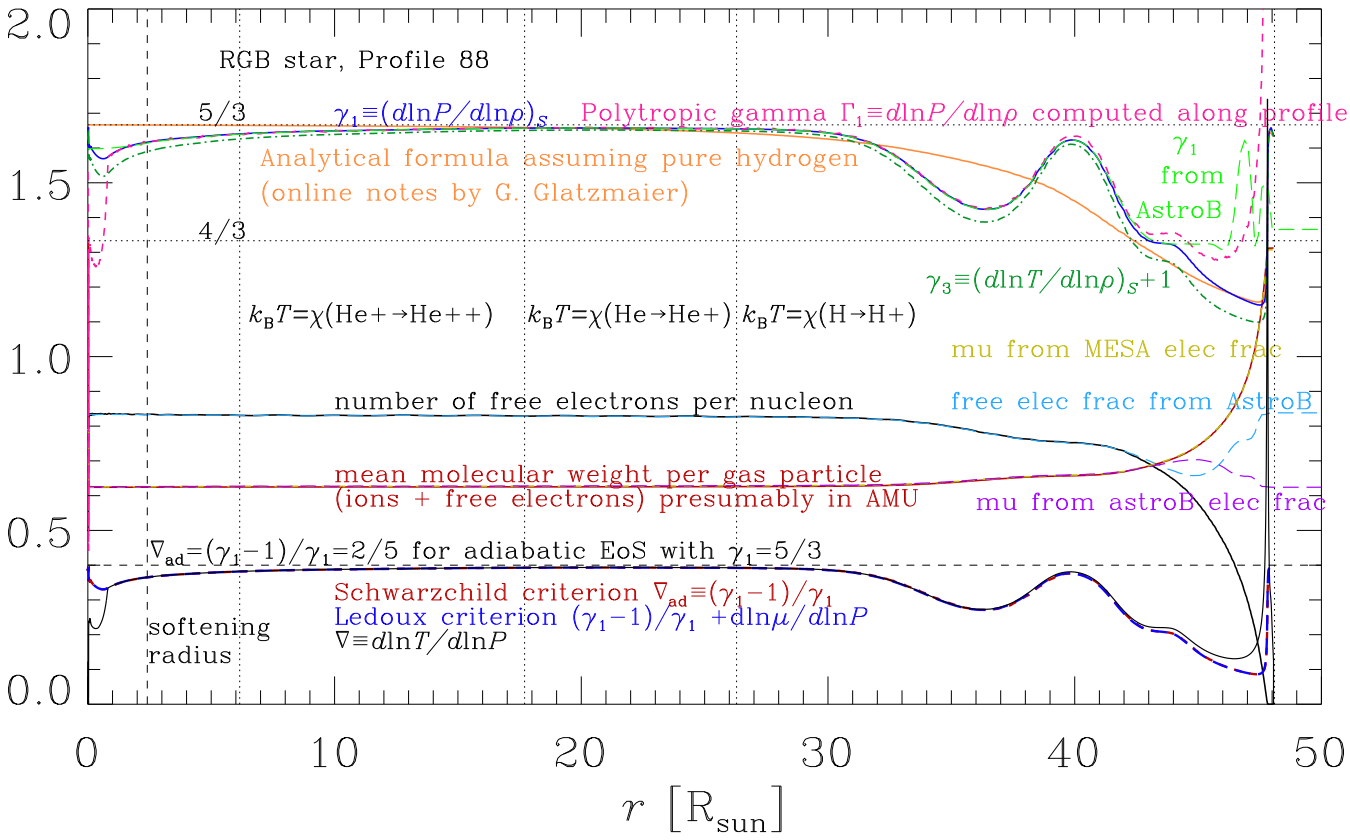

Figure 7. Graph showing Γ_1 (adiabatic index), free electron fraction and mean molecular mass profiles from MESA. We see that Γ_1 remains below 5/3 and dips below 4/3 near the surface. This behaviour is roughly predicted by an analytic model contained in the notes by G. Glatzmaier (lecture 6) that assumes pure hydrogen, using the free electron fraction profile from the MESA simulation, shown in black in the plot. We also see that $\Gamma_1 = (d\ln P/d\ln\rho)_S$ is quite similar to the polytropic $\gamma = d\ln P/d\ln\rho$ calculated for the stellar profile, which tells us that the envelope is probably convective. The electron fraction is fairly constant but dips after about $r = 30\,R_\odot$, which coincides with where μ increases. Finally we plot $\nabla = d\ln T/d\ln P$ and the critical value of $\nabla = d\ln T/d\ln P$ for (i) an ideal gas with $\Gamma_1 = 5/3$, which gives $(\Gamma_1 - 1)/\Gamma_1 = 2/5$, (ii) the MESA simulation neglecting the compositional gradient (Schwarzchild criterion) and (iii) the MESA simulation including the compositional gradient (Ledoux criterion). The plots below zoom in on this region to show more clearly what is happening as per convective stability/instability.

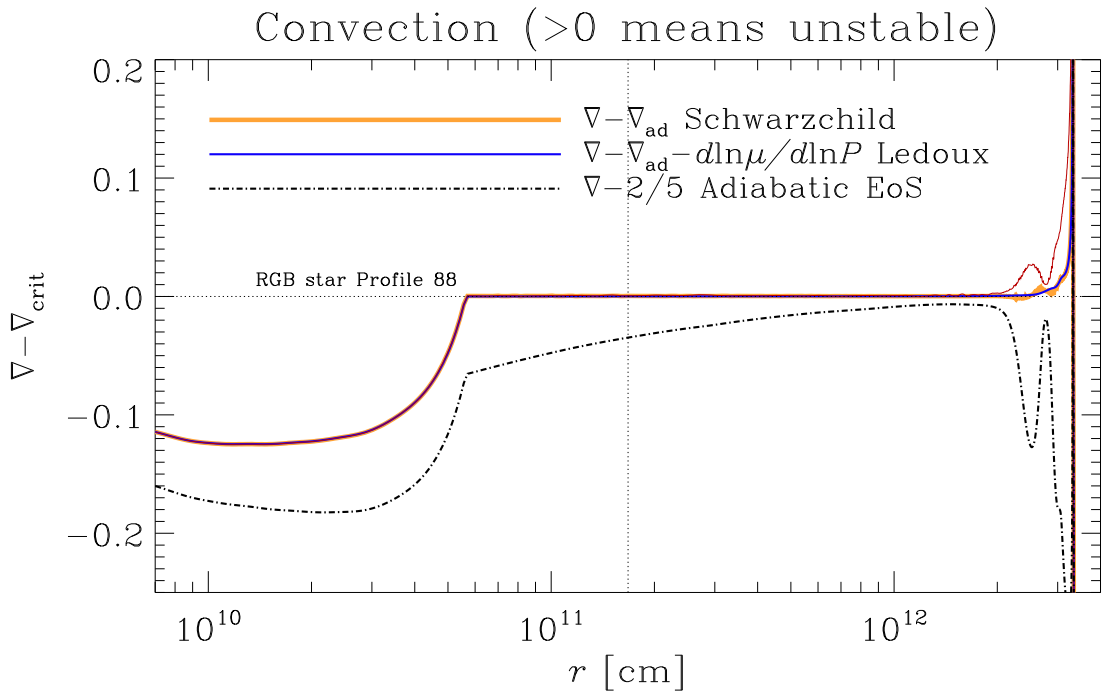

Figure 8. Graph showing condition for convective instability. This graph should be compared with Figure 6 (bottom left) from Ohlmann et al. (2017). Our results are consistent with theirs as long as we use the Ledoux condition outputted from MESA directly. If we compute the compositional gradient $d\ln\mu/d\ln P$ from μ and P we get the red line instead of the blue line. I don't understand why, but anyhow, as we will see in the next graph, both lines are consistent in that they predict convective instability. The black dash-dotted curve would be the relevant curve for the fiducial RGB simulation with adiabatic EoS ($\Gamma_1 = 5/3$). We see that for that simulation, the star is predicted to be convectively stable.

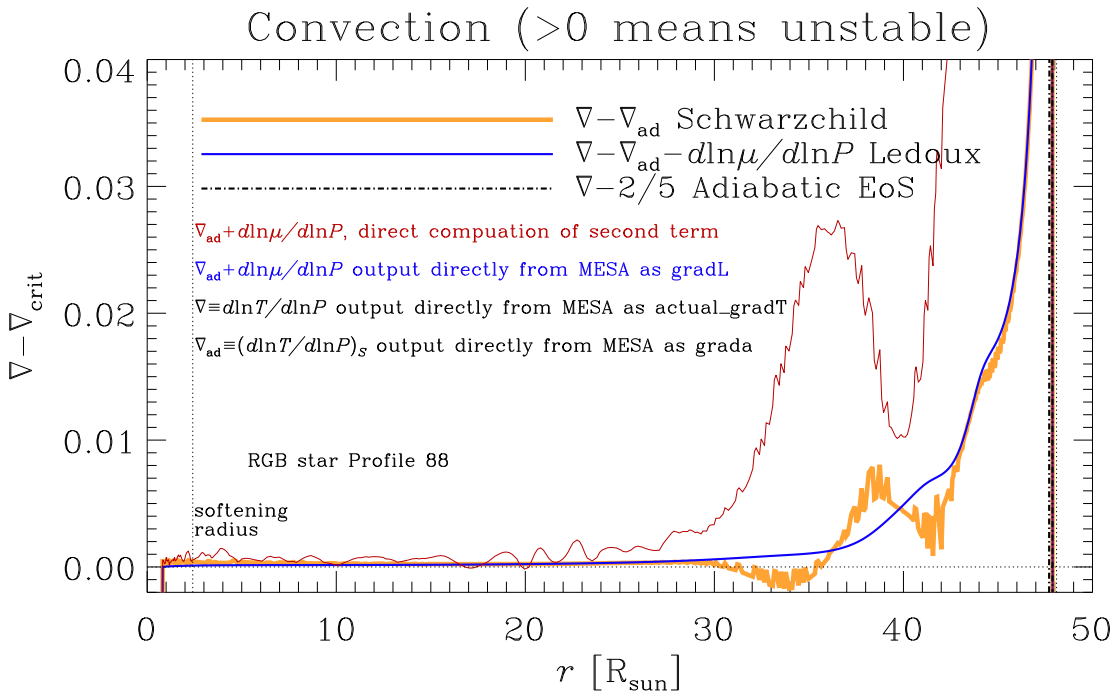

Figure 9. Graph showing condition for convective instability, plotted in a way that more clearly shows whether profile is stable or unstable. We clearly see that for the Ledoux criterion (blue line), which is the relevant criterion in our case, we are convectively unstable everywhere outside the softening radius. Note that the red line should match the blue line, but doesn't for some reason (see caption to Fig. 9), but in any case the red line also predicts convective instability. So to summarize, we see that the profile is convectively stable if the adiabatic $\Gamma_1 = 5/3$ EoS is assumed, but convectively unstable for the more realistic EoS, consistent with Ohlmann et al. (2017).

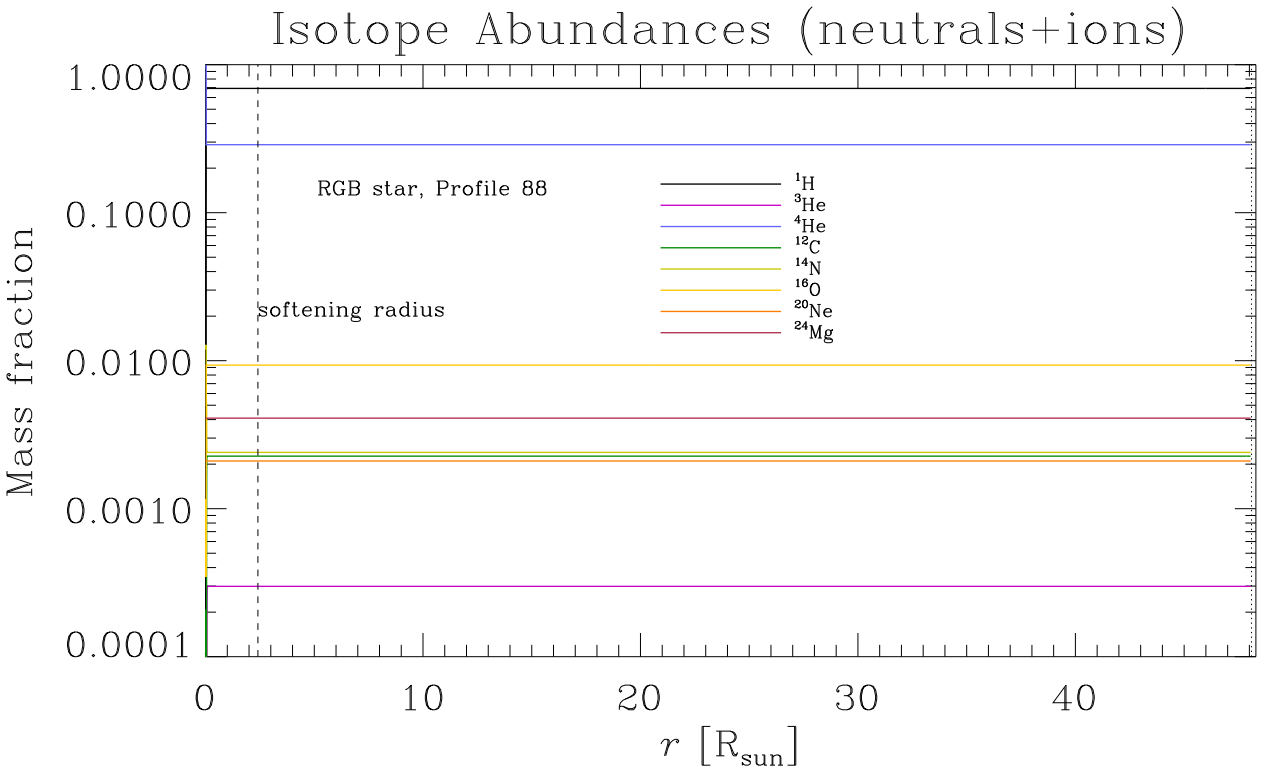

Figure 10. Mass fractions of the various isotopes available to be outputted by MESA.

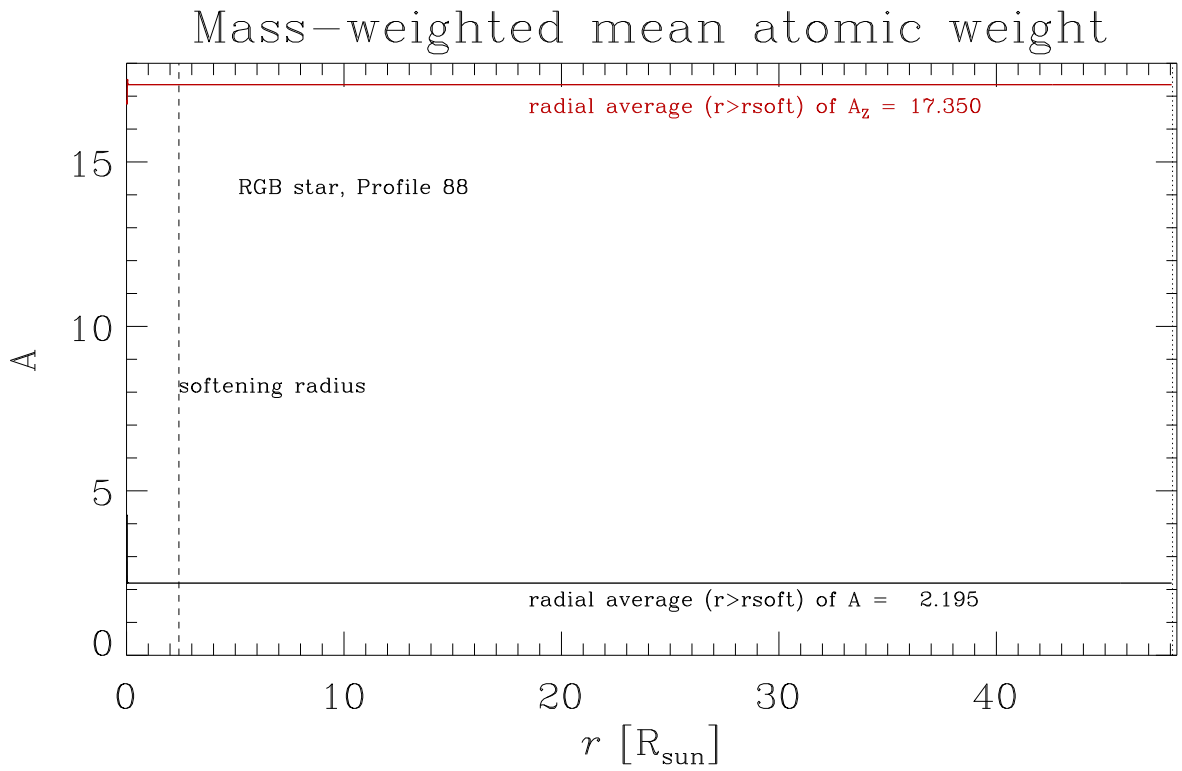

Figure 11. Mean atomic weight of metals above $r = r_{\rm soft}$, and mean atomic weight of all gas above $r = r_{\rm soft}$. Note that the former number is used in setting up the tabular EoS, but only for the part of the table where an ideal gas EoS is used. (Yisheng used $A_{\rm Z} = 18$ in his original table and for the Solar neighbourhood, $A_{\rm Z} \approx 15.5$.)

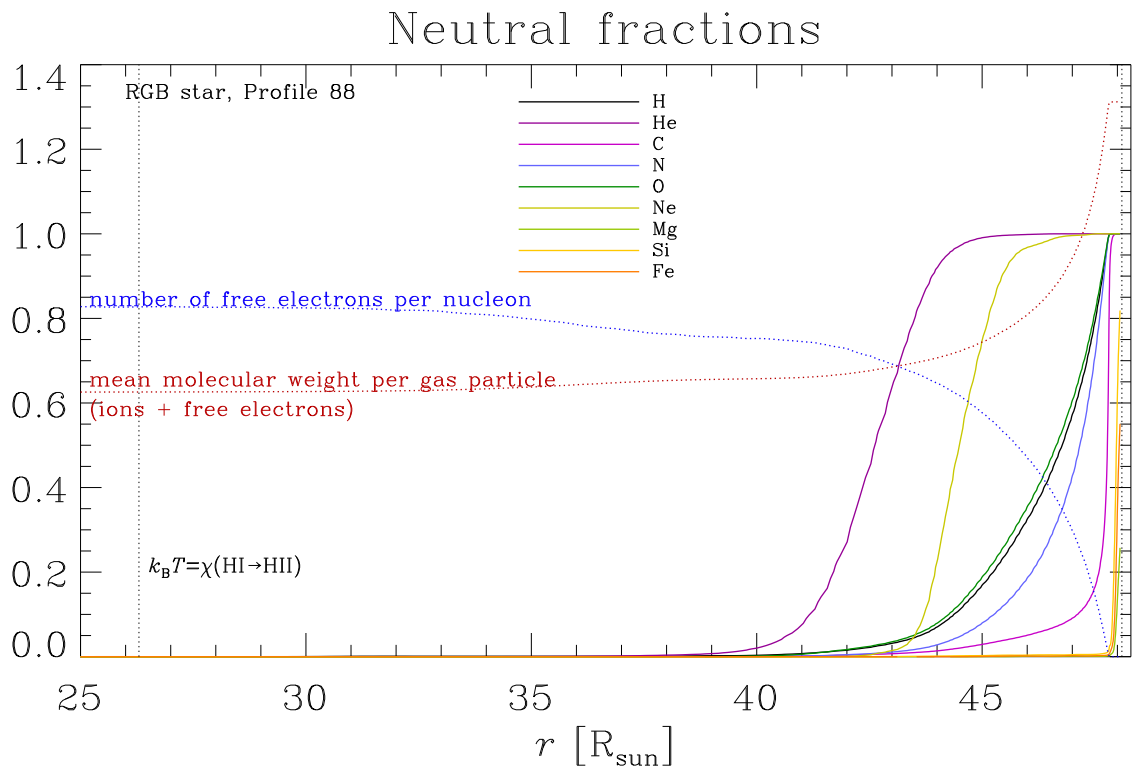

Figure 12. Neutral fractions as outputted by MESA (these do not come from the tabular EoS and so are estimated using more approximate physics). Adam suggests this figure could go in the paper. NOTE: have to check if He includes ^{3}He...

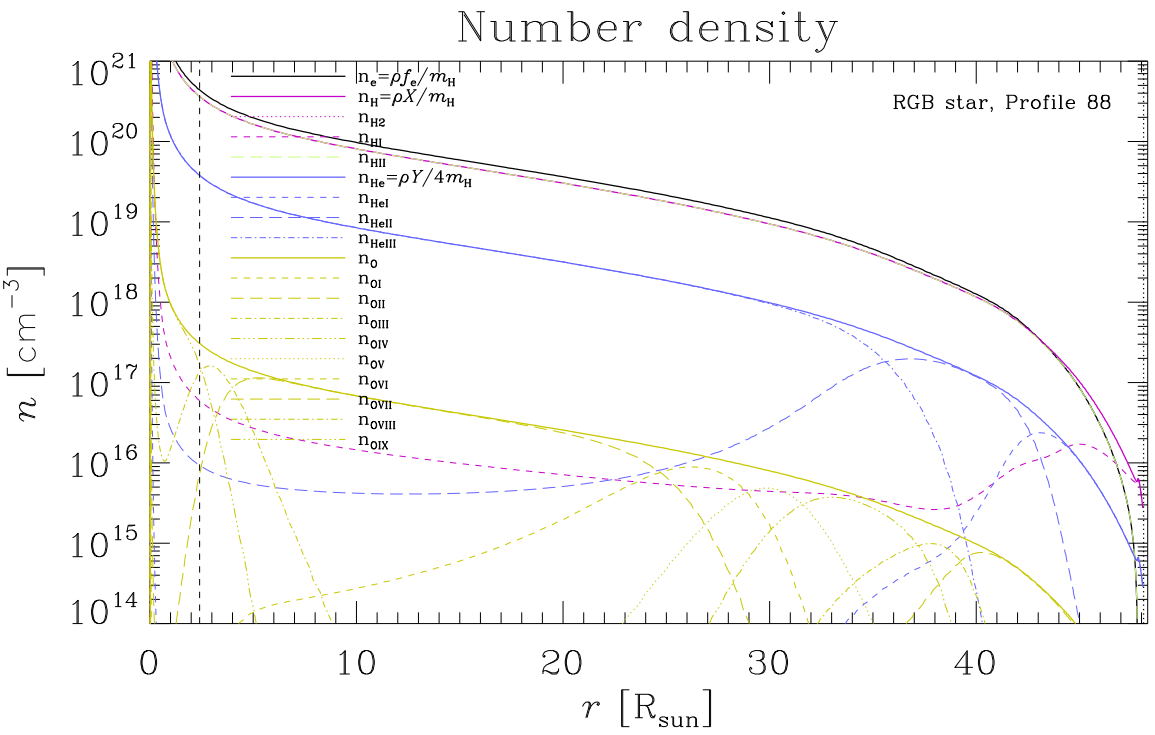

Figure 13. Number density of all the various ions. Here I included oxygen to avoid a messy plot but any of the metals can be plotted (that is, C, N, O, Ne, and Mg can be switched on or off in the plotting script). This was computed using the Saha equation (which is more approximate than the MESA EoS which is the OPAL EoS for this initial profile). In the Saha equation, the abundances of the various ions depend on the partition function. The partition function is equal to an integer for low temperatures (or apparently to 0.25 for H_2 but the number density of the latter is negligible anyway) but can rise very rapidly at high T above $\sim 10^4$ K. Here we use the $T \rightarrow 0$ limits but show the case of $T = 10^4$ K below.

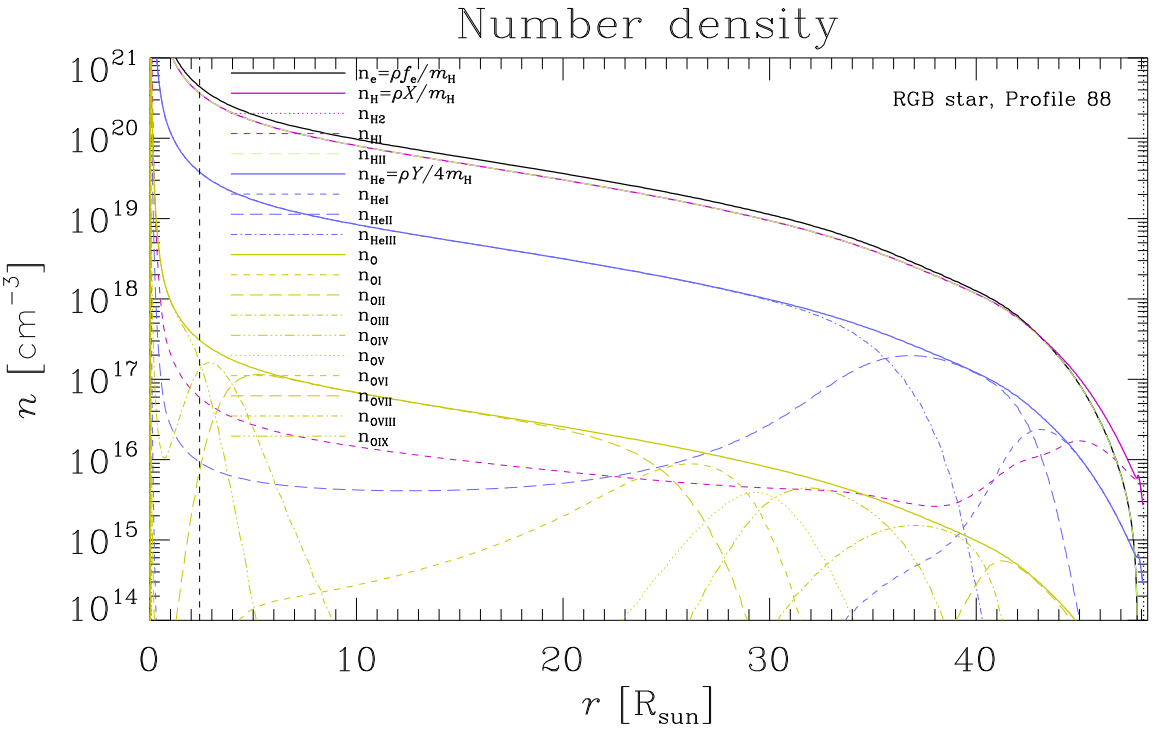

Figure 14. Same as Fig. 13 but now for partition functions computed using $T = 10^4$ K. Here I have inputted the values obtained from VizieR and NIST databases (the two databases are mutually consistent) because near the surface the approximate temperature is 10^4 K. This makes a small difference for the metals but the partition functions of H and He are not significantly affected.

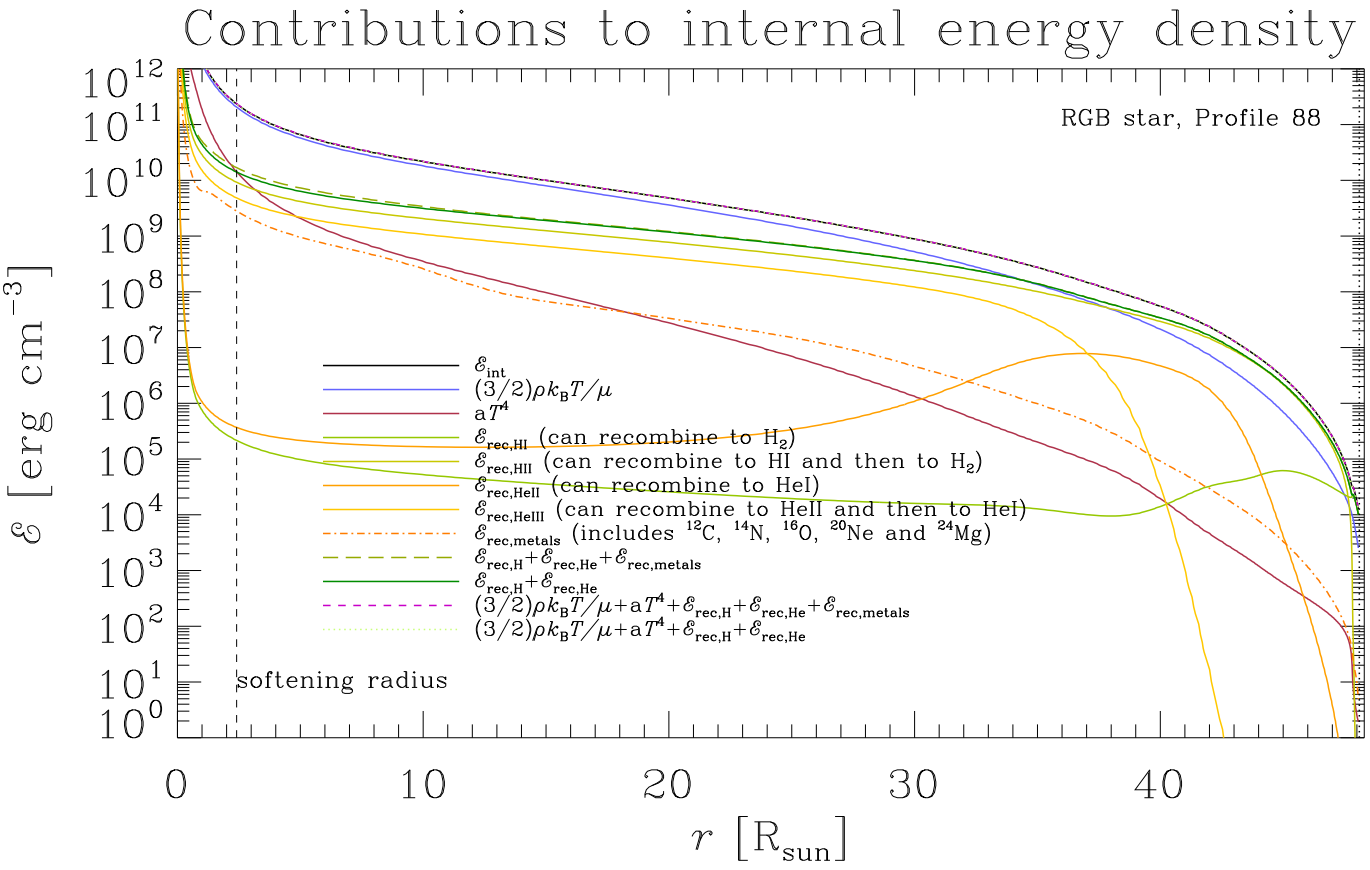

Figure 15. Internal energy contribution from different terms. Recombination energy is estimated using Saha equation. All ionic species of H, He, C, N, O, Ne and Mg are included. Note that there is a discrepancy near the surface between the internal energy density from MESA and that obtained by summing all the contributions. This suggests that the discrepancy near the surface is caused by some other missing physics, not recombination energy. Note that I have not tried looking at the temperature dependence of the partition function at higher temperatures, where hydrogen and helium partition functions are also affected. However, the numbers are such that the recombination energy froom H and He would be *reduced* if this were included. Moreover, it is not clear whether those database results are accurate for stellar atmospheres, particularly since no pressure/density dependence is given in the databases.

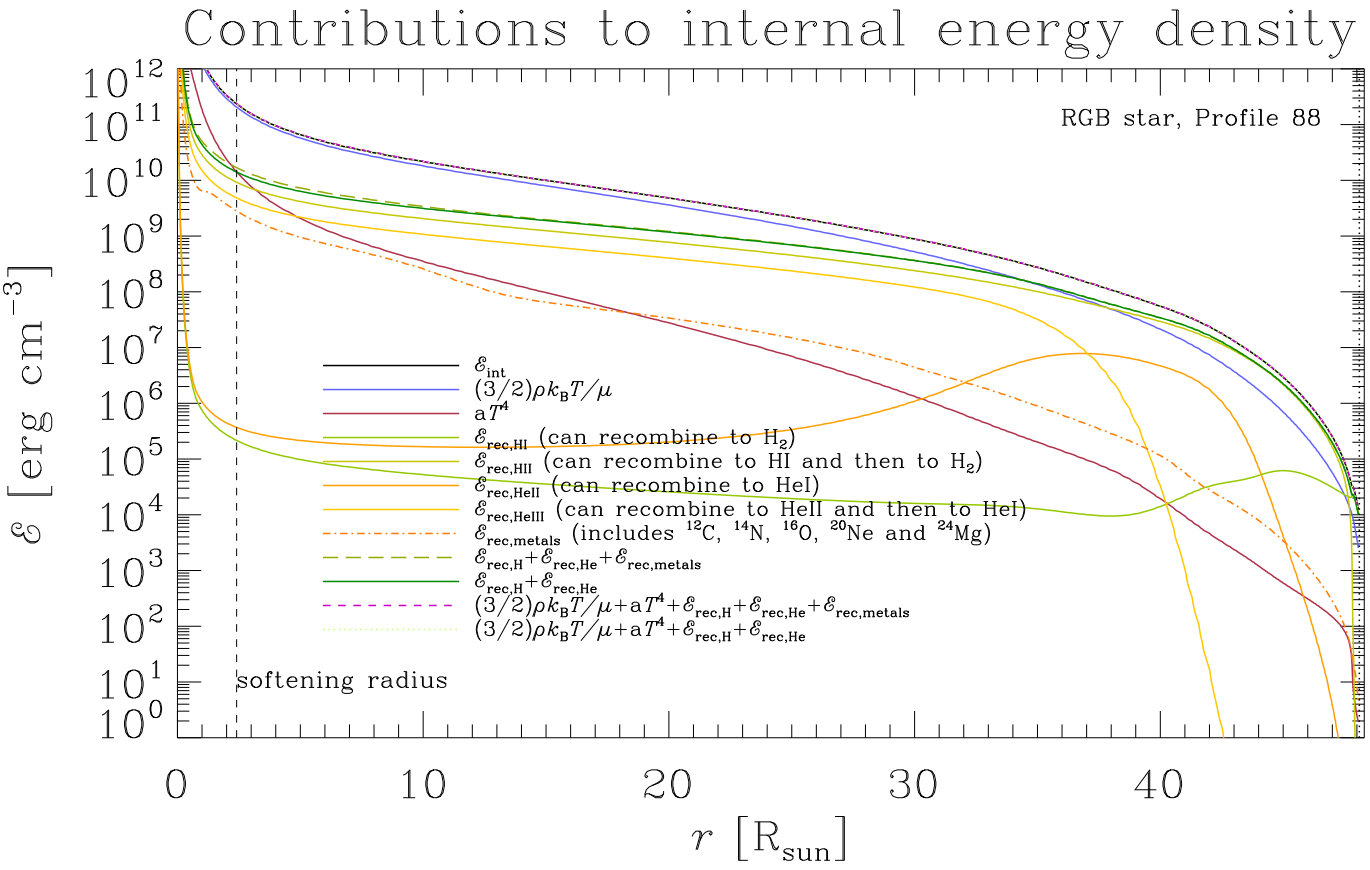

Figure 16. Same as Fig. 15 but now for $T = 10^4$ K. The recombination energy from metals change slightly. Using the $T = 10^4$ K partition function values from VizieR and NIST databases alters the metals contribution slightly but does not affect the hydrogen and helium contributions. Since the metals contribution to the recombination energy is negligible anyway, this does not matter.

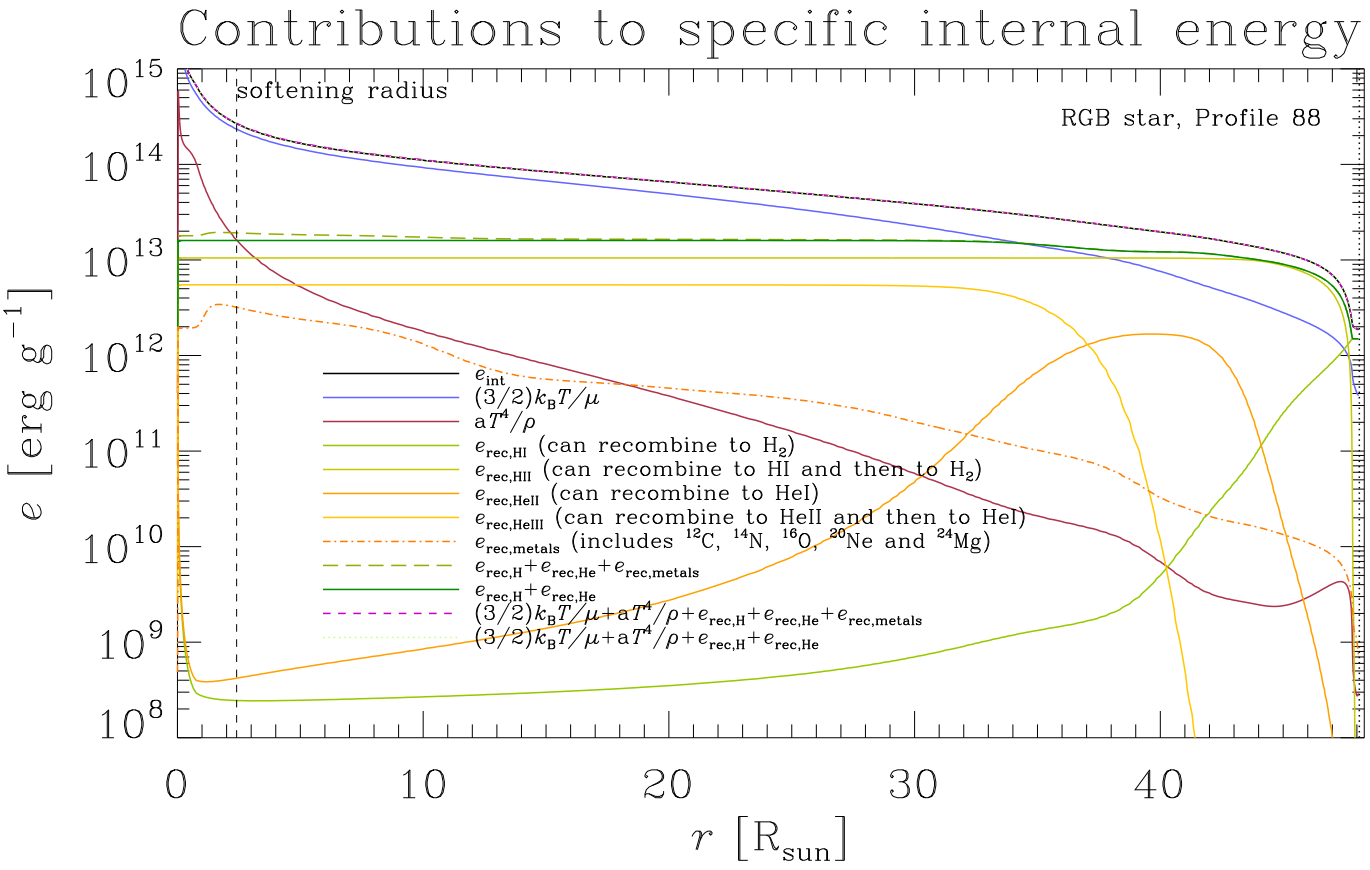

Figure 17. Similar to Fig. 15 but now showing the *specific* internal energy.

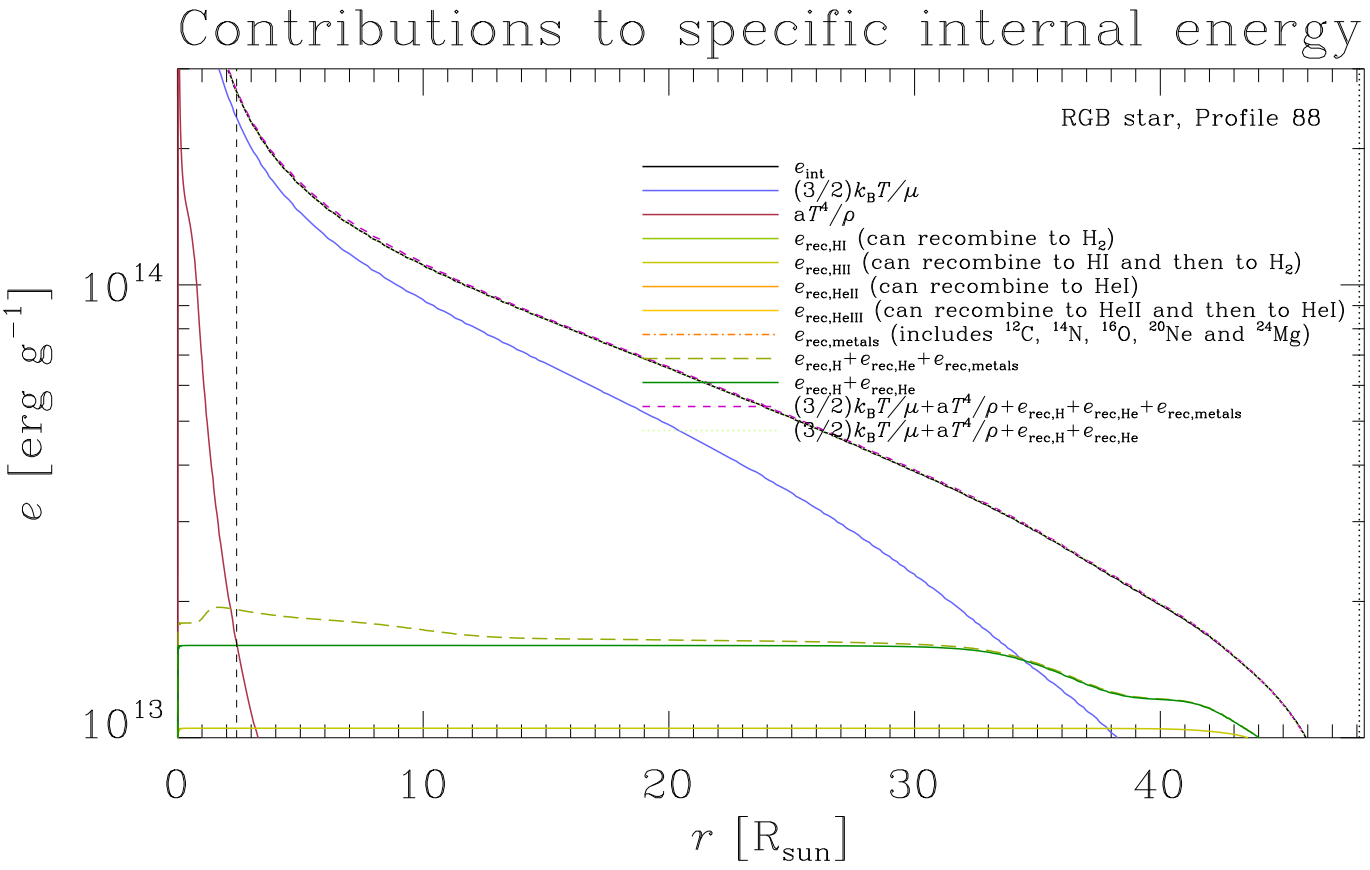

Figure 18. Similar to Fig. 17 but now zooming in. We see that by including the hydrogen and helium contributions to the recombination energy, the MESA specific internal energy is reproduced almost perfectly.

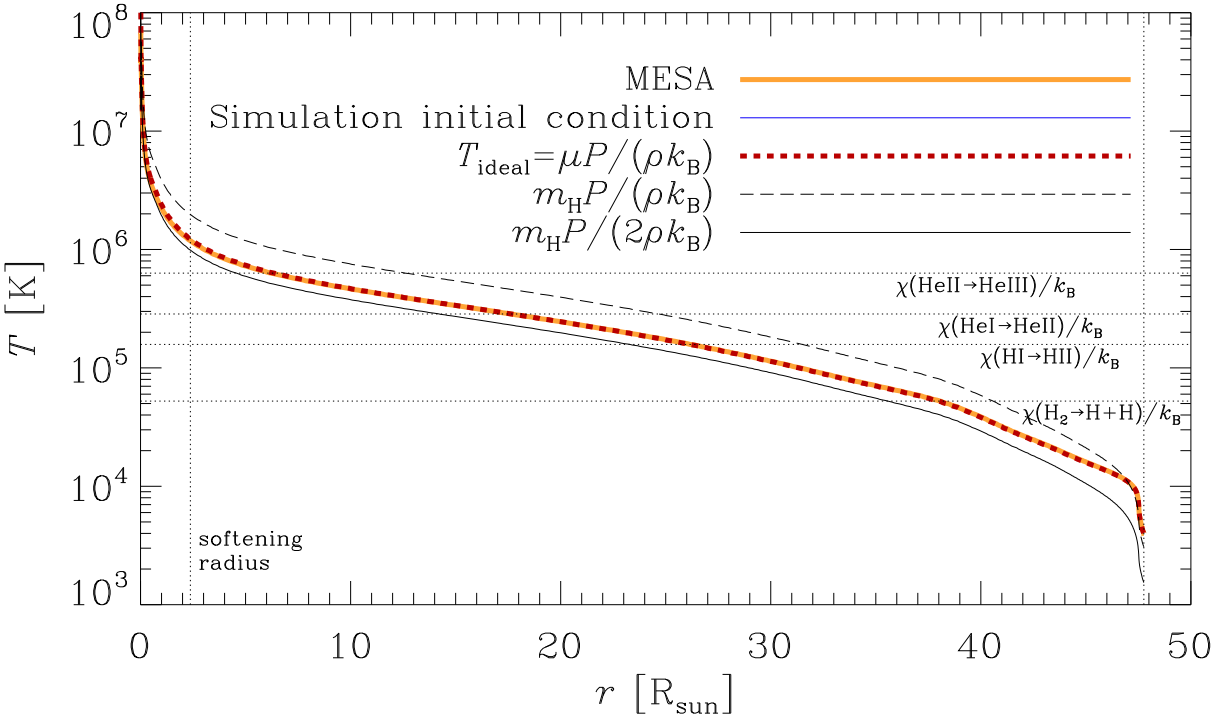

Figure 19. NOW FOR SIMILAR TIME SNAPSHOT BUT USING MESA RELEASE 12778 INSTEAD OF 8845. THIS WAS DONE TO MAKE SURE THAT NEW EOS REFINEMENTS IN MESA DID NOT AFFECT THE RESULTS. NOTE THAT THE 8845 SNAPSHOT IS IN BETWEEN TWO SNAPSHOTS SO I TOOK THE ONE CORRESPONDING TO THE TIME JUST PRIOR TO THE 8845 SNAPSHOT. THE MAIN RESULT IS THAT EVERYTHING IS AS EXPECTED, CONSISTENT WITH 8845, SO WE CAN CONTINUE TO USE 8845.

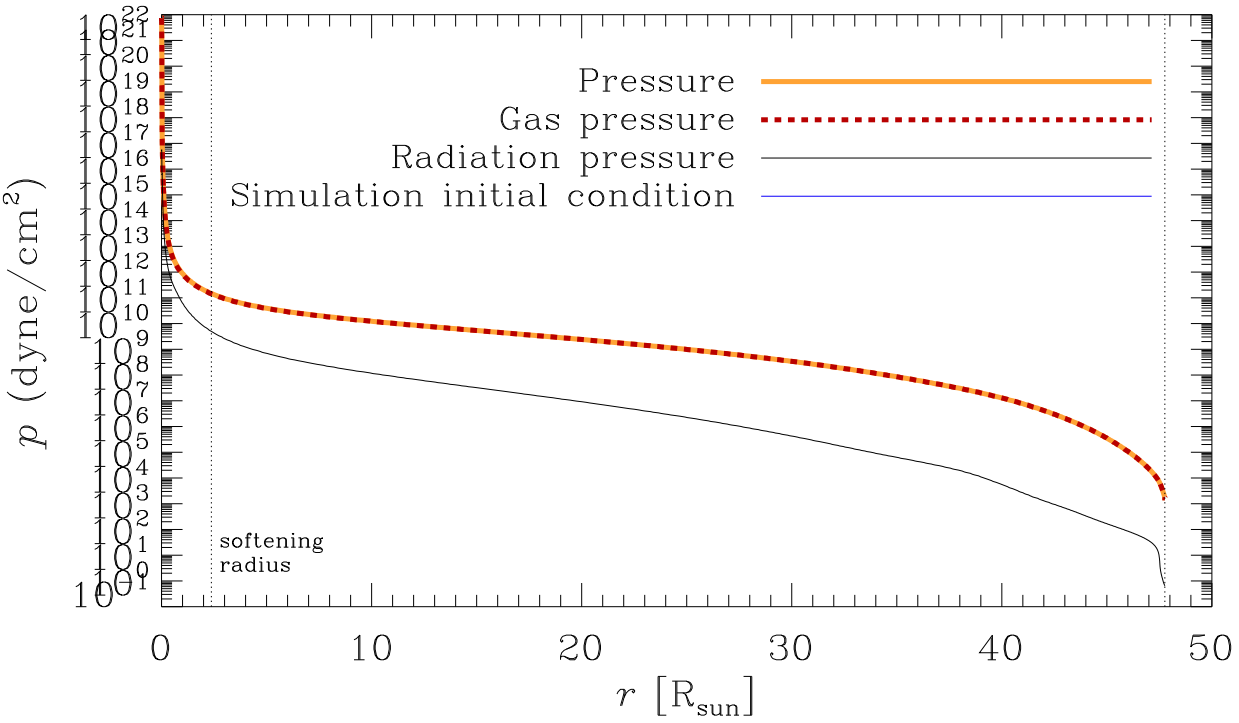

Figure 20. MESA r12778.

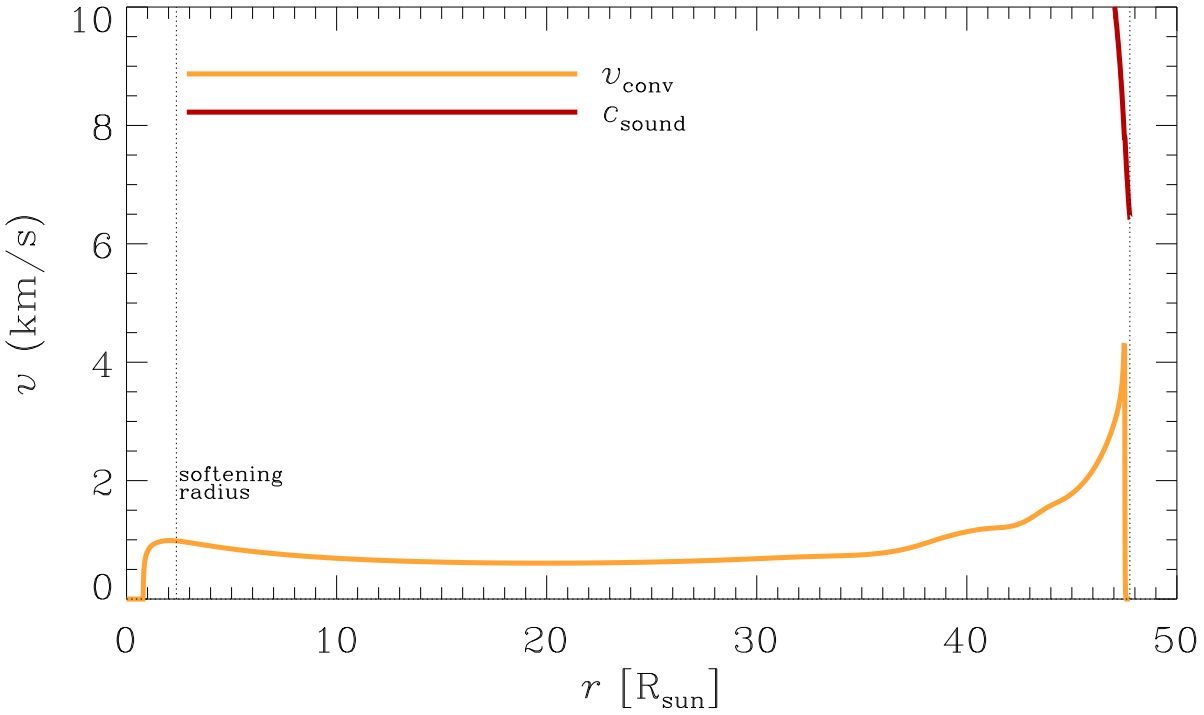

Figure 21. MESA r12778.

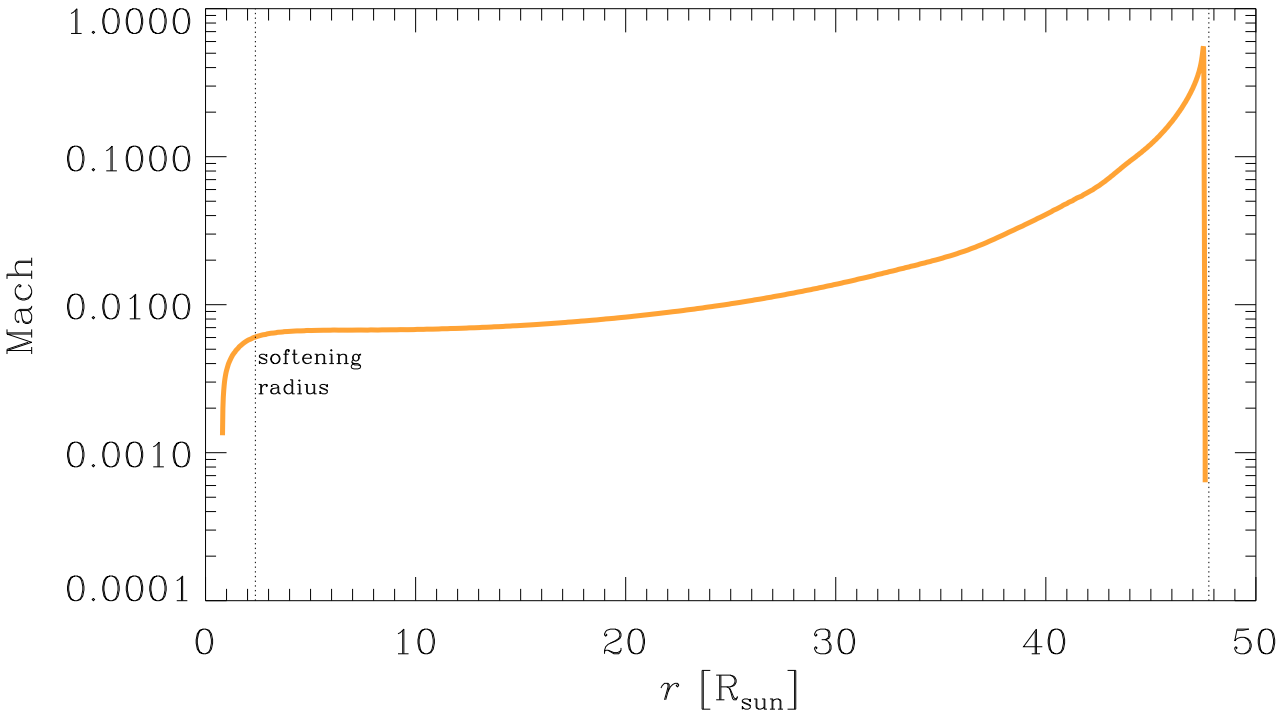

Figure 22. MESA r12778.

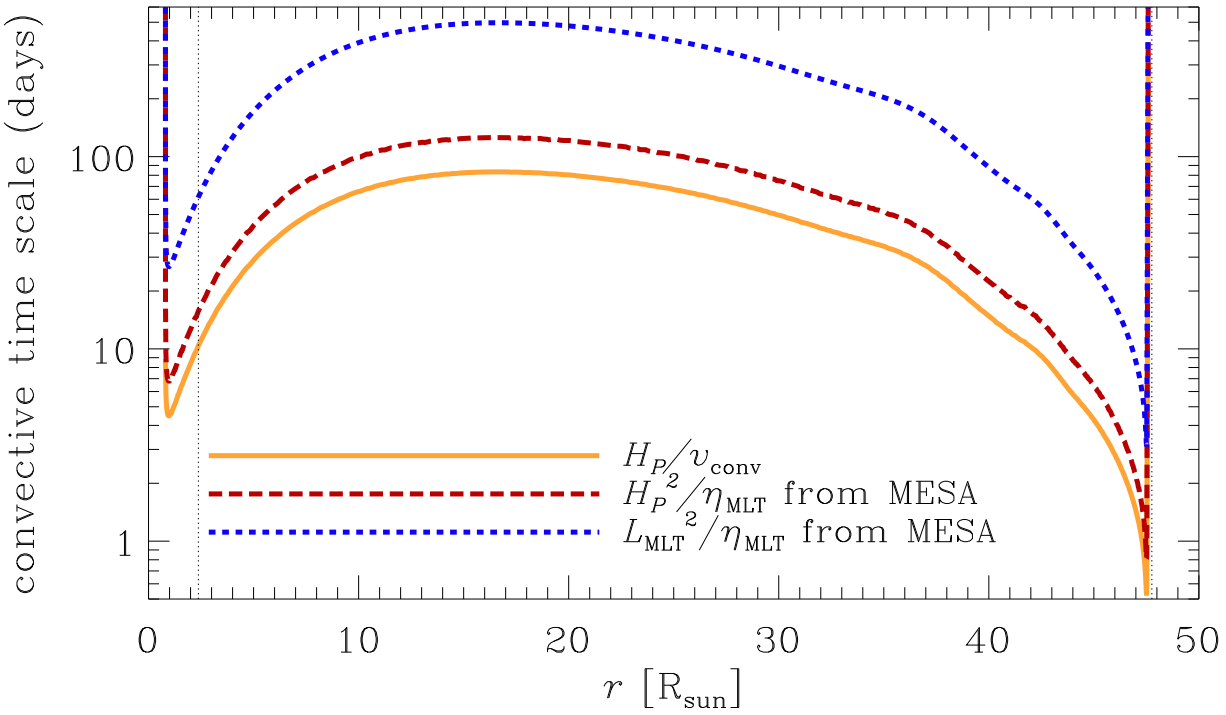

Figure 23. MESA r12778.

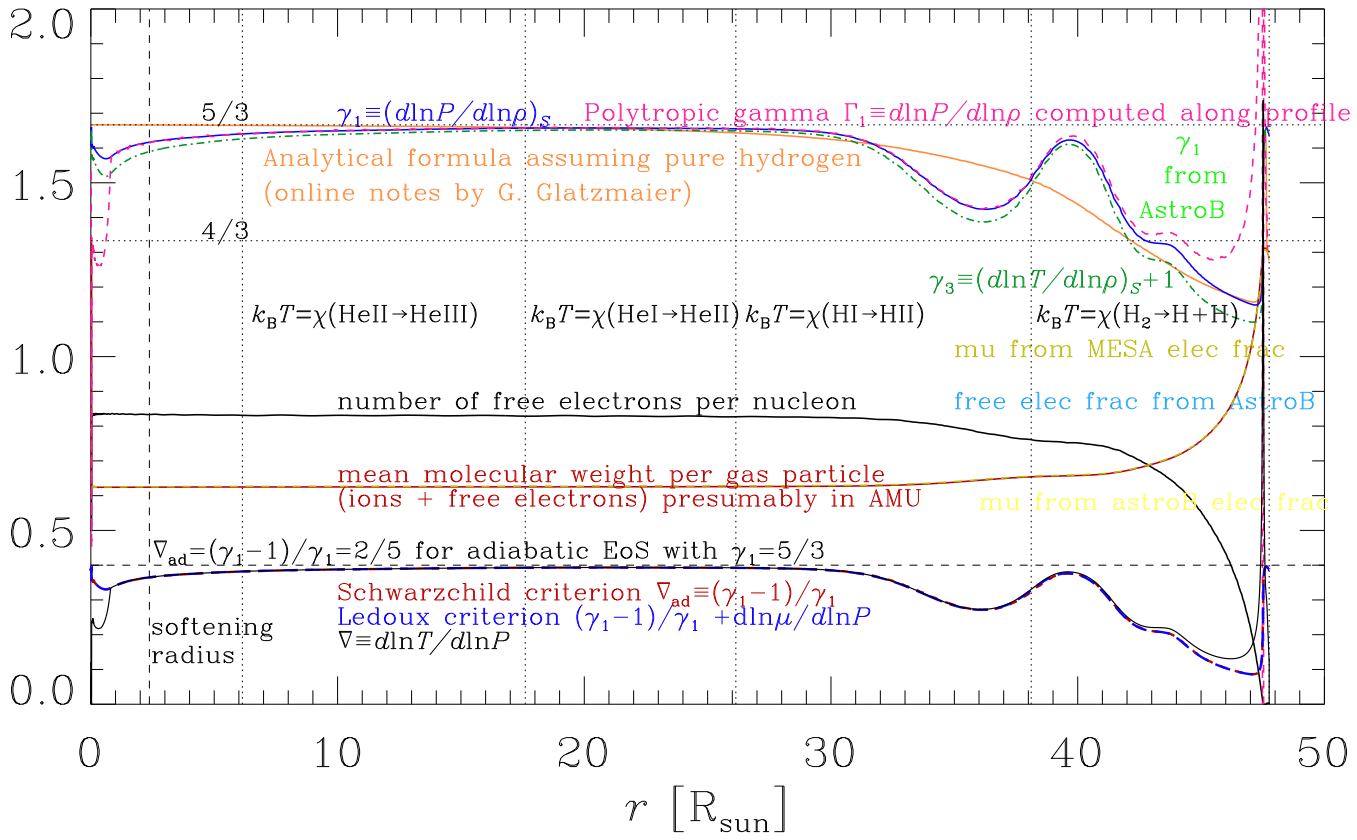

Figure 24. MESA r12778.

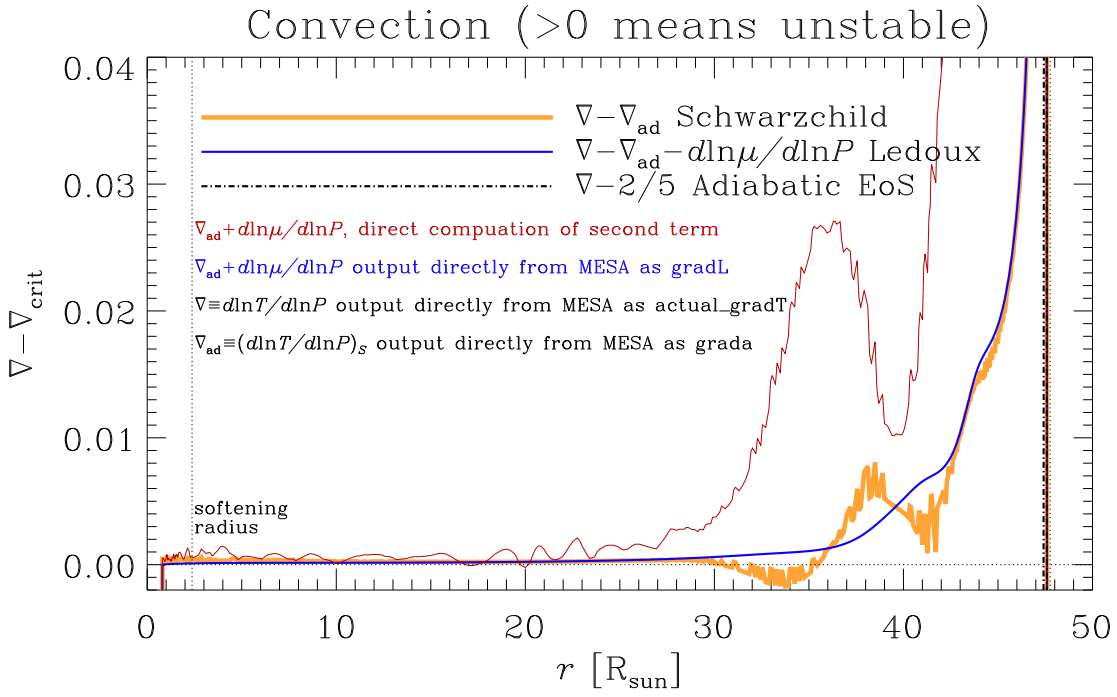

Figure 25. MESA r12778.

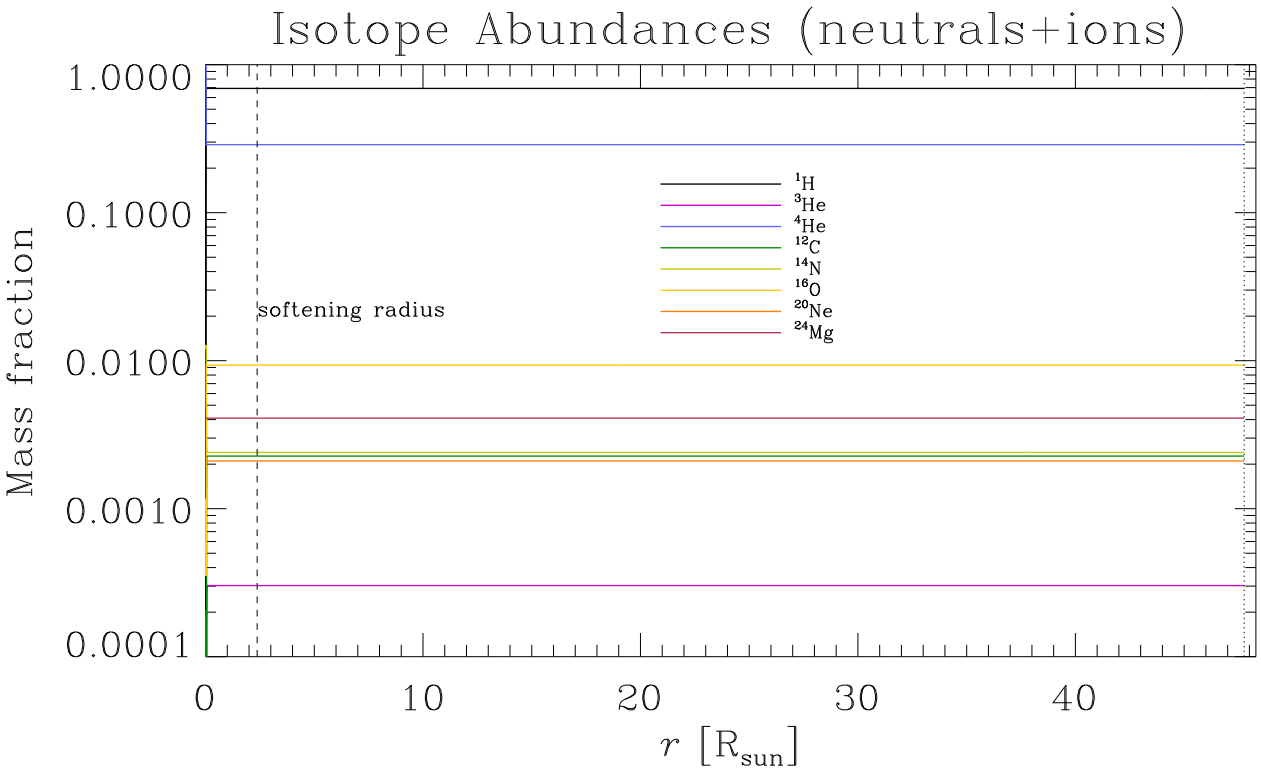

Figure 26. MESA r12778.

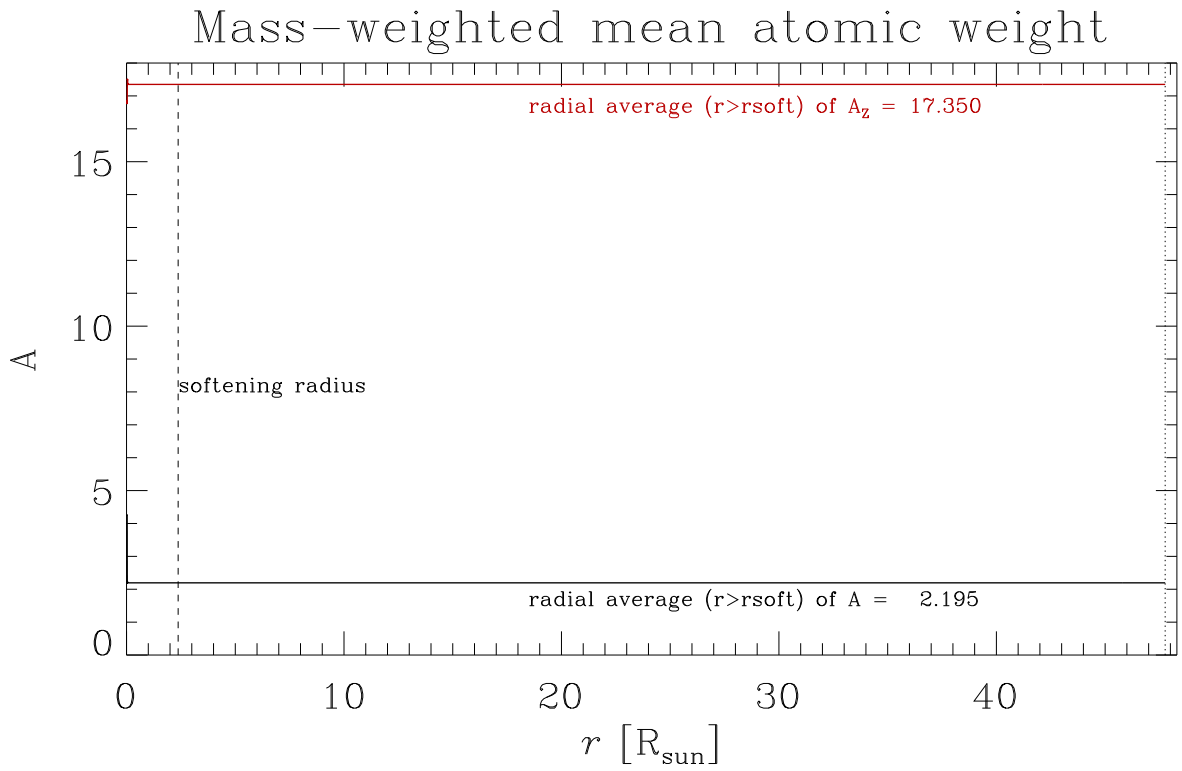

Figure 27. MESA r12778.

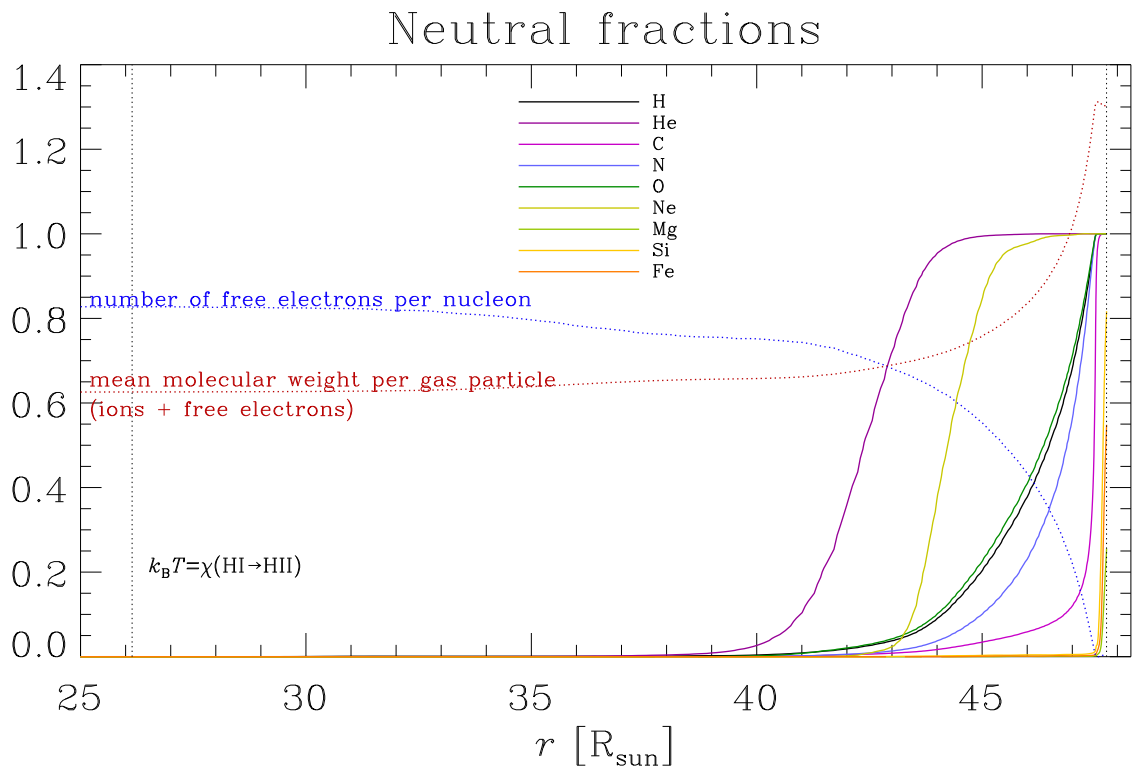

Figure 28. MESA r12778.

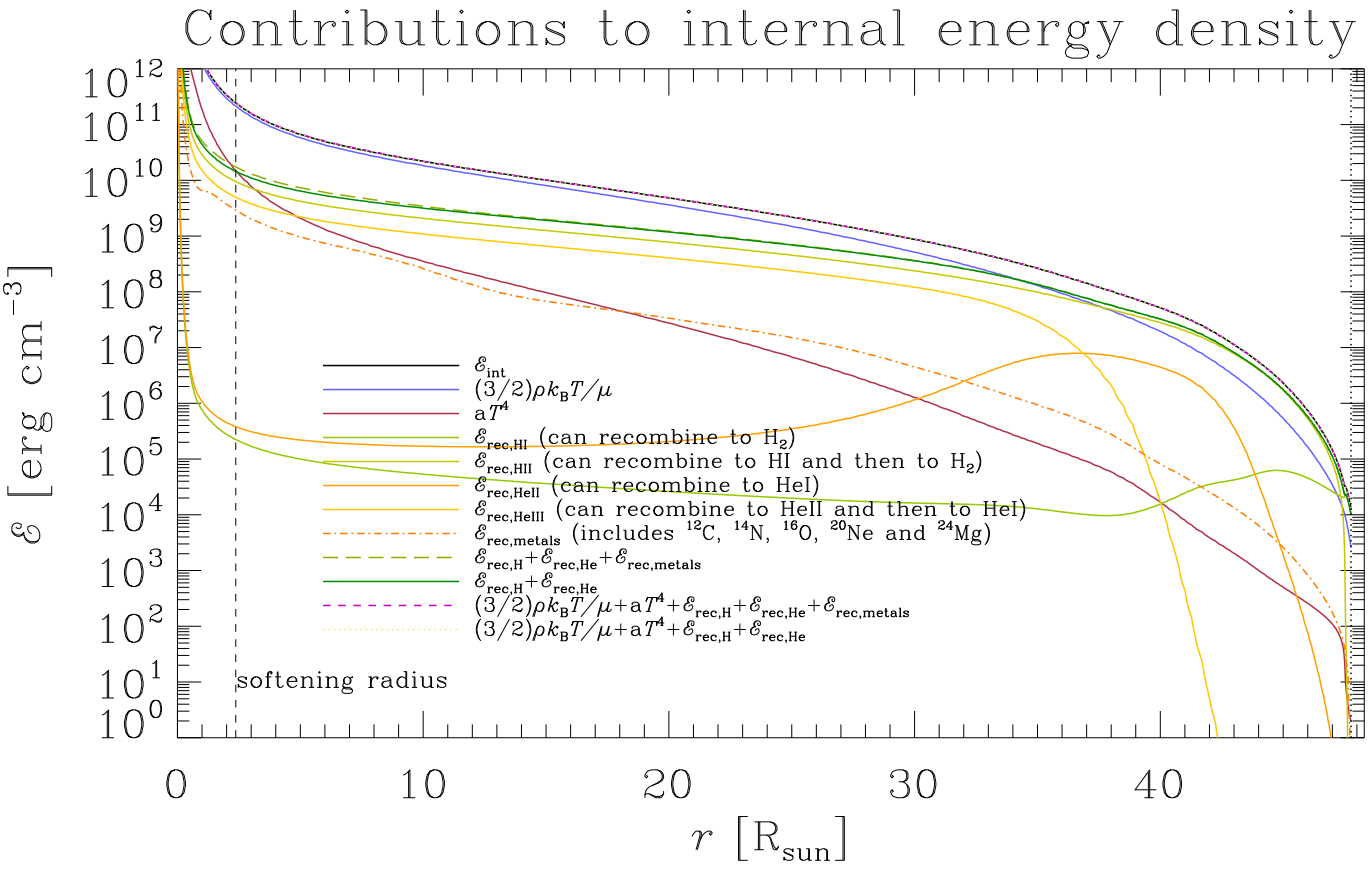

Figure 29. MESA r12778.

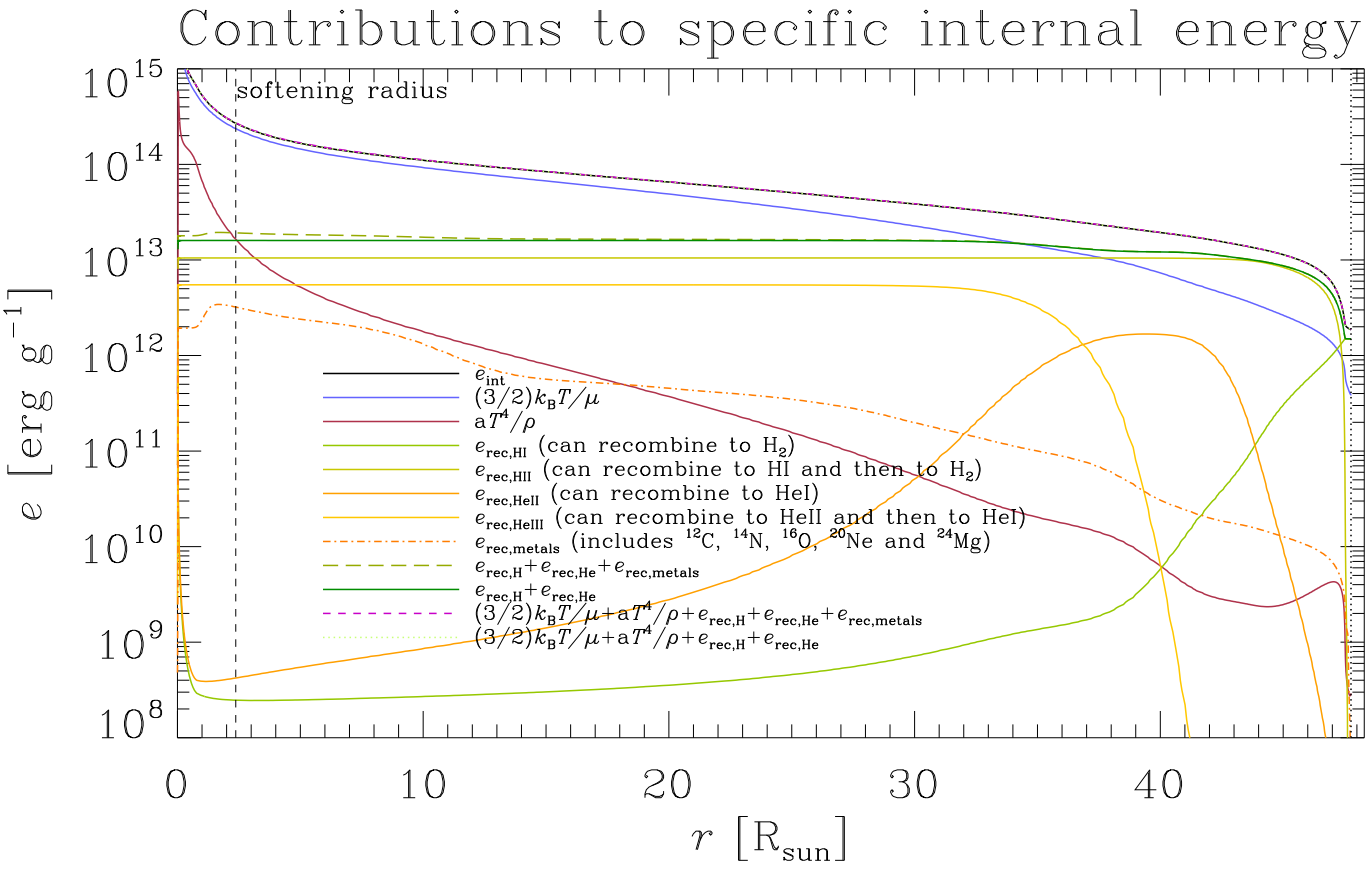

Figure 30. MESA r12778.

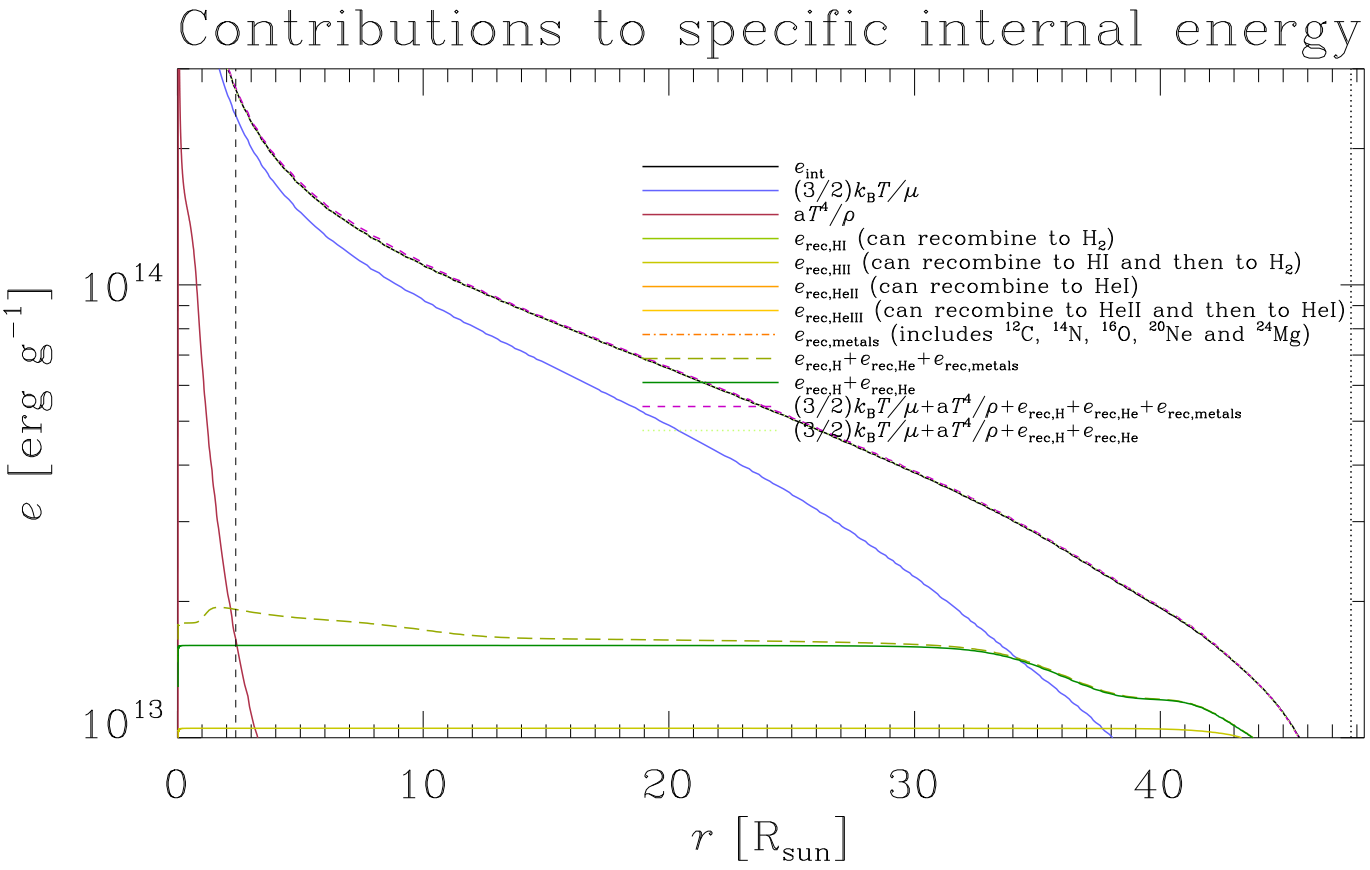

Figure 31. MESA r12778.